



# Advances in Colloidal Quantum Dot-Based Displays for QLEDs and Patterning Applications

Awais Ali<sup>1</sup> · Seongkeun Oh<sup>1</sup> · Woosik Kim<sup>1</sup> · Soong Ju Oh<sup>1</sup>

Received: 29 April 2024 / Revised: 30 July 2024 / Accepted: 3 August 2024

© The Author(s), under exclusive licence to Korean Institute of Chemical Engineers, Seoul, Korea 2024

## Abstract

Various display devices utilize colloidal quantum dots (QDs) for photoluminescent (PL) and electroluminescent (EL) applications owing to their exceptional optical properties, including sharp emission bandwidths, tunable emissions spectra, and photoluminescence quantum yields approaching unity. Since the commercialization of PL-based devices, researchers have shifted focus to the commercialization of EL-based devices and patterning processes. Over the past decade, the performance of EL devices has been dramatically enhanced through the meticulous optimization of the device architecture. In addition, solution-based QD patterning techniques have advanced, offering methods that minimize damage to the coated QDs while preserving their intrinsic properties effectively. Recent innovations include the development of ink formulations that improve the stability of QDs under ambient conditions and the use of photolithographic and soft lithographic techniques to achieve high-resolution patterning. This article reviews the recent advancements in various EL-based devices and solution-based methods for QD patterning, highlighting their potential to enable more complex, multi-color displays, and their implications for next-generation consumer electronics.

**Keywords** Colloidal quantum dots · Electroluminescence · Light emitting · Patterning · Printing diodes

## Introduction

In recent years, quantum dots (QDs) have garnered significant attention as representative examples of nanoparticles owing to their remarkable attributes and versatile applications [1, 2]. QDs are nanoscale semiconductor particles that exhibit quantum confinement effects, which give rise to size-tunable electronic and optical properties [3–5]. This intrinsic tunability, coupled with their high photoluminescence quantum yield and broad absorption spectrum, has made QDs promising candidates for diverse optoelectronic devices, including displays, solar cells [6], sensors [7–11], and photodetectors [12–16]. In display technology, researchers have utilized QDs as conversion materials in photoluminescent (PL) devices and as self-emitting layers

in QD-electroluminescence (EL) devices [17]. Since the commercialization of PL-based devices, researchers have shifted their focus to EL-based devices [17].

However, a major issue arises because of the low device performance caused by limitations in the device architecture and fabrication techniques [18]. Although the external quantum efficiency (EQE) approaches the theoretical limit of +20% for RGB based on Cd/Cd-free QDs, the challenge remains to further improve the device performance for commercialization [19]. The low efficiency of these devices is attributed to the complexity of the multilayer structure of QLEDs and poor fabrication techniques [18]. A typical QLED structure comprises transport layers for electrons and holes and an emission layer [20]. One of the key factors causing low device performance is the mismatch in the energy levels between these layers [21]. Various techniques, such as doping transport materials and exploring new materials, have been employed to address this issue [22].

Related to fabrication, it is imperative to fabricate high-resolution pixels based on QLEDs and similar QD-based light-emitting components [23–31]. However, the conventional photolithography processes commonly used for patterning can compromise the excellent optical

---

Awais Ali and Seongkeun Oh contributed equally.

✉ Soong Ju Oh  
sjoh1982@korea.ac.kr

<sup>1</sup> Department of Materials Science and Engineering,  
Korea University, 145, Anam-ro Seongbuk-gu, Seoul,  
Republic of Korea

properties of QDs. Therefore, there is a demand for the development of new patterning process technologies that can maintain the characteristics of quantum dots while enabling the fabrication of high-resolution patterns. Recent developments in quantum dot patterning technologies have revealed several trends: (i) methods such as quantum dot surface modification to mitigate the drawbacks of photolithography-based patterning; (ii) direct photopatterning techniques that utilize light irradiation directly onto quantum dot films with added photosensitive materials, inducing selective property changes without the need for photoresist (PR); (iii) inkjet printing methods in which patterns are formed by directly depositing solution droplets; and (iv) transfer printing techniques in which quantum dots are transferred onto substrates in patterned forms.

This review addresses these issues by focusing on QLED device architecture and detailing various layers, including the emission, electron, and hole transport layers. The fabrication process includes various techniques, including photolithography, photopatterning, inkjet printing, and transfer printing.

## Device Structure of QD-LEDs

The device structures of QLEDs typically fall into two categories, conventional and inverted [32], as shown in Fig. 1(a). In the conventional structure, the arrangement of layers involves arranging an ITO anode, a hole injection/transport layer (HIL/HTL), an emission material layer (EML), an electron transport layer (ETL), and an Al cathode [21]. Conversely, the inverted structure involves the arrangement of an ITO cathode, ETL, EML, HTL, HIL, and Al anode, as shown in Fig. 1(b). In conventional structures, researchers commonly use poly(3,4-ethylenedioxythiophene):poly(styrenesulfonate) (PEDOT:PSS) as the HIL in Cd-free QLEDs [33]. PEDOT:PSS minimizes the energy barrier between the HIL and the anode by adjusting the work function [34]. The hydrophilic and acidic nature of PEDOT:PSS causes corrosion of the ITO electrodes, which affects device stability [35]. To address this issue, Zhao et al. employed inorganic metal oxides as HILs for Cd-free QLEDs in 2022, aiming to enhance device stability [36]. They used dual HIL by incorporating  $\text{NiO}_x$  and Mg-doped  $\text{NiO}_x$  that boosted the performance of Cd-free QLEDs; the maximum EQE increased from 7.6% to 11.2%, and the device stability was enhanced seven times using dual HIL [36]. The device performance of inorganic metal oxide-based HIL lags behind that of

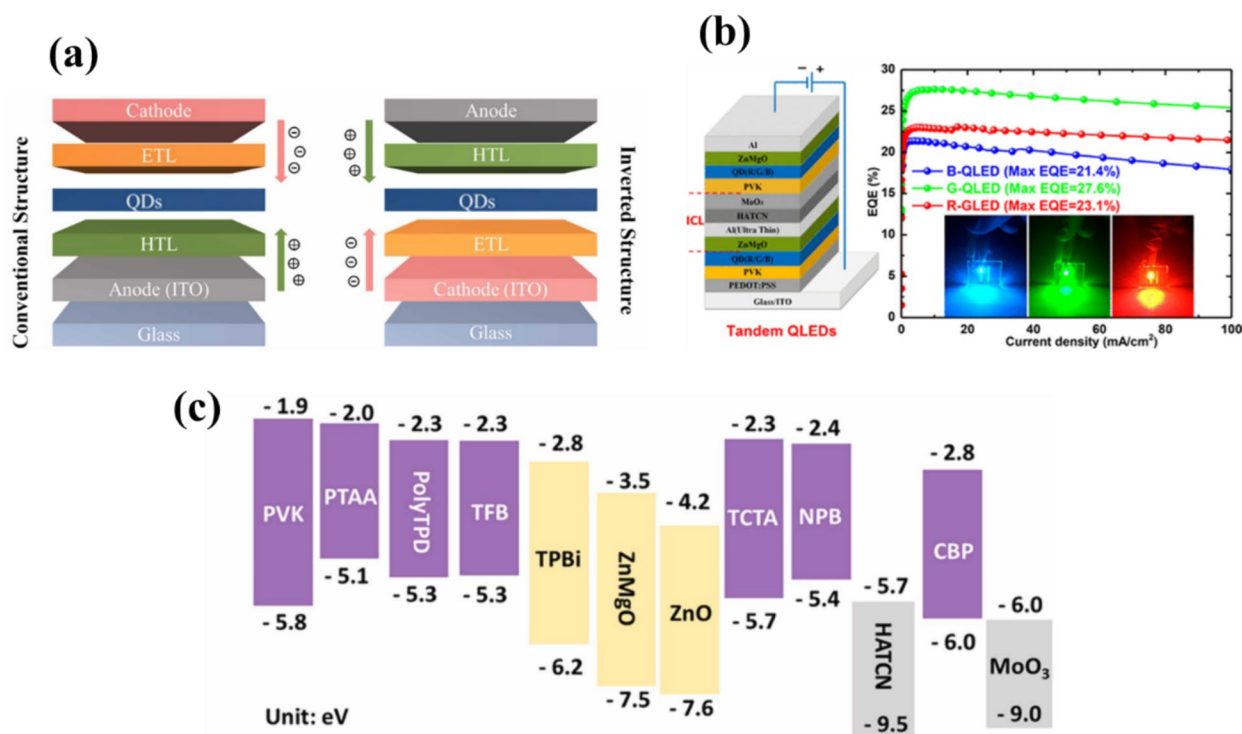


**Fig. 1** **a** QLEDs structure (conventional and inverted) Copyright © 2022 Wiley-VCH GmbH [32], **b** tandem QLED structure [42] Copyright © 2018, American Chemical Society, and **c** energy levels diagram of the generally used HTL, Copyright © 2020, American Chemical Society [32]

PEDOT:PSS-based QLEDs, indicating the need for further investigations of inorganic metal oxide HILs. In inverted device structures, inorganic  $\text{MoO}_3$  and organic HATCN are commonly used as HIL materials, whereas organic TCTA, TAPC (4,4'-cyclohexylidenebis[N,N-bis(4-methylphenyl)benzenamine]), and CBP are frequently used as HTL [37]. In the inverted device structure, the HIL and HTL were prepared almost exclusively using high vacuum thermal evaporation [38]. This technique prevents solvent erosion during film deposition in the multilayer solution process. In 2016, Kim et al. enhanced the electroluminescence (EL) performance of QLED using double HTL, TAPC, and CBP [39]. When CBP was used for the HTL, the EL peaks of the device displayed an unwanted spectrum in the dark blue region, primarily because of the significant injection barrier between the HTL and EML. In addition, the deep LUMO level failed to efficiently prevent electron flow, causing exciton recombination within the HTL [40]. Alternatively, substituting CBP with shallow-level TAPC as the HTL eliminated undesired emissions and resolved the issue of uneven carrier injection in the device [41]. In addition to conventional and inverted structures for enhancing the EQE of QLEDs, Zhang et al. [42] developed a tandem structure in red, green, and blue QLEDs, achieving a notable EQE of over 21% by combining two or more QD-LED units in series, as illustrated in Fig. 1b. A transparent interlayer connecting layer (ICL) was used to link multiple QD-LED devices [42]. The resulting device showed high EQE and current efficiency of 23.1% and 41.5 cd/A, 27.6% and 121.5 cd/A, and 21.4% and 17.9 cd/A for red, green, and blue QLEDs, respectively. Figure 1c shows an energy level diagram of common QLEDs [43]. The carrier mobility and energy level were the primary parameters for the selection of each functional layer. Alternatively, the charge transport characteristics of each functional layer can be tuned by adjusting the thickness of each layer [21].

### Recent Progress in Emitting Layer

Initially, different QD materials were studied, including CdSe [44, 45], GaAs [46], ZnSe [47], InP [48], and PbS [49]. Owing to their high brightness and coverage of the entire visible range, CdSe-based QDs are the most prominent [50]. As a restriction from Restriction of Hazardous Substances (RoHS) in 2002, six hazardous materials were banned, including cadmium (< 100 ppm). However, they offer six different reagents with high reactivities [51]. Therefore, alternatives for efficient Cd-based QLEDs have attracted the attention of researchers, and InP-based QDs are considered the best candidates for displays among all alternatives because of their small full width at half maximum (FWHM) and non-toxicity [51]. However, other than InP, some Cd-free QDs are also introduced like perovskite

quantum dots (PQDs) [52],  $\text{CuInS}_2$  [53], and Ag-In-Ga-S QDs [54]. PQDs offer excellent luminescence properties, they often suffer from poor stability and susceptibility to moisture and oxygen, which can degrade their performance over time, are known for their low toxicity and tunable emission spectra [21],  $\text{CuInS}_2$  are known for their low toxicity and tunable emission spectra, but they generally have lower photoluminescence quantum yields (PLQY) compared to other QDs, which can limit their brightness and efficiency, and Ag-In-Ga-S QDs provide a broad absorption spectrum and high PLQY, their synthesis can be complex and costly, which may hinder their widespread commercial adoption. All these limitations make the InP more interesting. Researchers have consistently reported improvements in luminescence and QD-LED applications using InP core/shell quantum dots [55–58]. Jiang et al. synthesized multi-shelled InP-based QDs using a safe and inexpensive phosphorus source  $(\text{DMA})_3\text{P}$  (tris(dimethylamino)phosphine), and post-treatment with hexanethiol (HT) improved the QY from 71 to 81.8% [22]. Figure 2a shows that surface treatment with HT enhanced the intensity of the PL spectra, demonstrating the suppression of surface-defect traps due to the passivation of the QDs. In 2020, Kim et al. enhanced the QY of green QDs and reported that with zinc oxo clusters, QDs with a narrow FWHM of 37 nm and a high PLQY of 95% can be synthesized [59]. The analysis results in Fig. 2b show that the two different functions of zinc oxo clusters can improve the optoelectronic properties: (1) defects were successfully controlled by the formation of an oxidized buffer layer, and (2) swift injection of a highly reactive phosphorus source induced size uniformity of the In(Zn)P core. Similarly, the use of reactivity-controlled precursors is an effective method for synthesizing well-controlled QDs [60]. Won et al. also removed surface defects using HF etching during mid shell (ZnSe) growth, which produced a more spherical shape [61]. A 100% PLQY was obtained using spherical InP/ZnSe/ZnS QDs. The InP-based QLED achieved a theoretical EQE limit of approximately 20% and a high operational performance, rivaling the performance of the top Cd-based QLEDs, as illustrated in (Fig. 2c).

### Recent Progress in ETL

Owing to their negligible electron injection barrier and high electron mobility, ZnO nanoparticles have become the most widely used ETL materials [63, 64]. High electron mobility causes an unbalanced charge injection in the device [65]. Although the transport properties of ETL can be varied by optimizing the layer thickness and particle size of ZnO, exciton quenching at the layer interface can occur because defects on the surface of ZnO nanoparticles can trap excitations and cause radiation centers [66]. It has been reported that doping ZnO with different materials can adjust

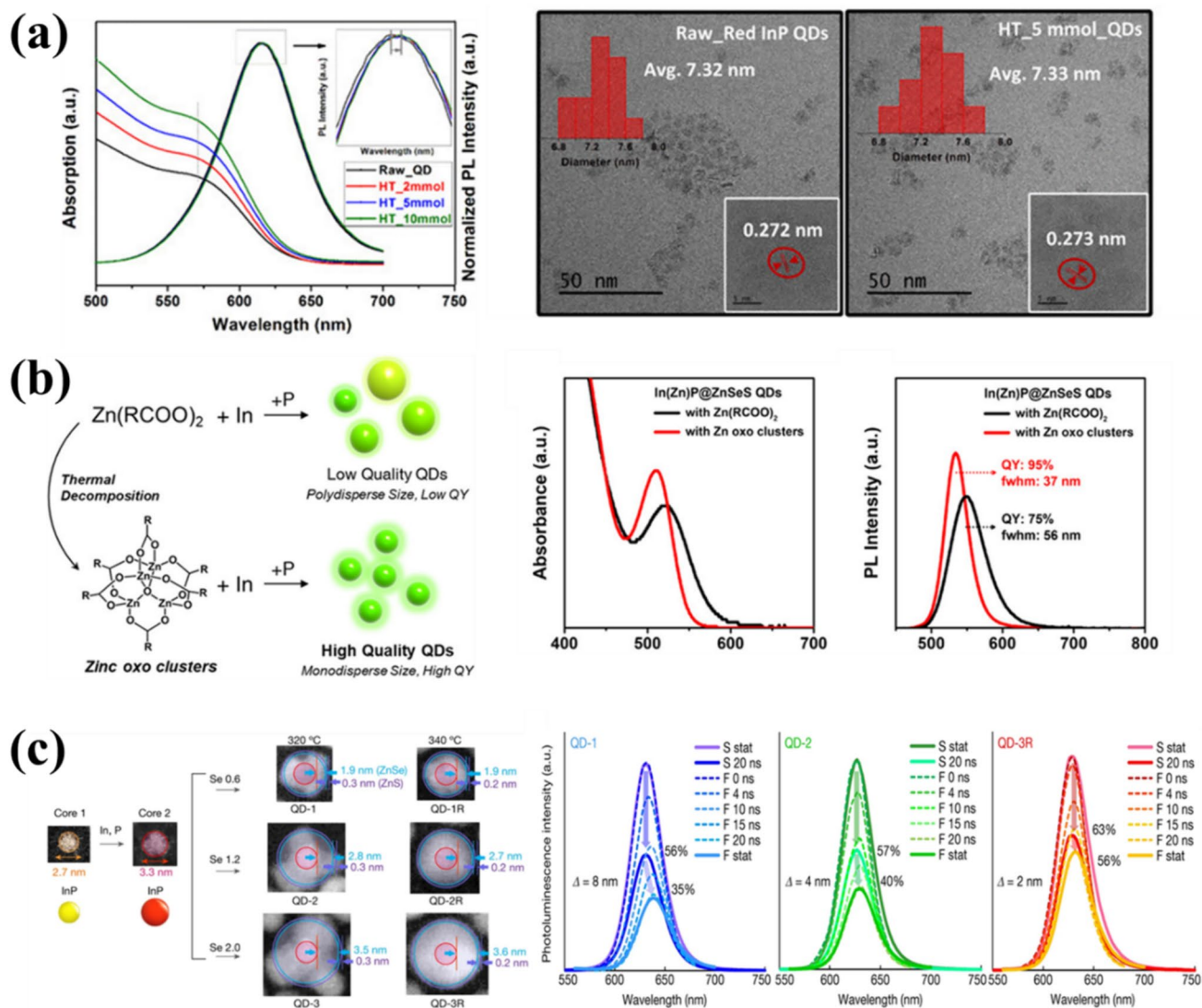


**Fig. 2** **a** PL and UV–Vis absorption spectra of  $(\text{DMA})_3\text{P}$ -based InP QDs with HRTEM images (inset W/O HT treatment), Copyright © 2020, American Chemical Society [22], **b** Quality difference of synthesized InP-based QDs with different zinc reagent, along with UV–

Vis absorption and PL spectra, Copyright © 2020 American Chemical Society [59], and **c** (left) STEM images of InP cores with different shell thickness (Right) PL spectra of QD film, Copyright © 2019, The Author(s), under exclusive license to Springer Nature Limited [62]

the energy levels, which can reduce electron mobility. Fei Chen et al. compared the doping effect of different metallic components with those of ZnO nanoparticles [61], as shown in Fig. 3a. Cd-free QLED devices have been fabricated using different ZnO-based ETLs doped with ZnO:In, ZnO:Mg, or ZnO:Li. Doping ZnO with Mg metal ions shifted the energy level upward, enhancing electron injection and reducing electron accumulation at the layer interface. Electron-only devices (EODs) data showed that the doping of ZnO with different metal ions caused a reduction in electron mobility, and ZnO:Mg-based ETL showed the best performance. The defect states on the surface of ZnO:Mg NPs were removed by Cl passivation, which further improved the maximum brightness of the device to  $5,595 \text{ cd/m}^2$  and the

EQE to 4.24%. The Mg-doped ZnO nanoparticles exhibited the best performance. In 2017, Wang et al. determined the effect of Mg-doped ZnO nanoparticles on a Cd-free QLED, which increased the brightness of the QLED to more than  $10,000 \text{ cd/m}^2$  [67]. Moon et al. in 2019 reported that the excess of electrons in Cd-free QLEDs is the main reason for the non-radiative recombination process, and they found the effect of different concentrations of Mg-doped ZnO ETL and a maximum brightness of  $13,900 \text{ cd/m}^2$  and EQE of 13.6% reported with a 12.5 mol% Mg ZnO ETL [68]. From another perspective, Wu et al. argued that the enhancement of Cd-free QLED using Mg-doped ZnO as the ETL resulted from the passivation of the band gap states and a decrease in the electron conductivity. Even the Mg doping reduced

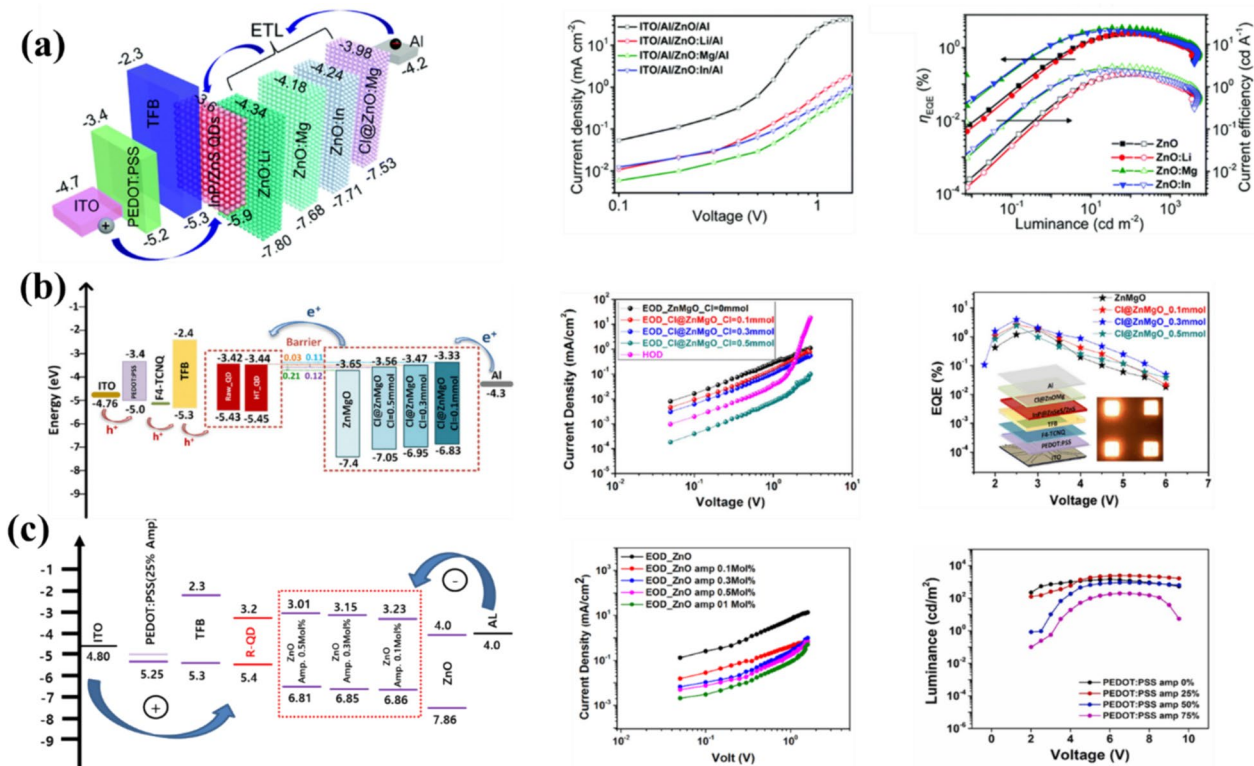


**Fig. 3** **a** QLEDs with energy levels (left),  $J$ - $V$  characteristics of the different EOD (based on different ETLs) (right) Copyright © 2023 Elsevier B.V. All rights reserved., [49], **b** QLEDs with energy levels (left), [22], Copyright © 2020, American Chemical Society and

QLEDs with energy levels (left),  $J$ - $V$ ,  $J$ - $V$ - $L$  characteristics of the different EOD and QLEDs (based on different ETLs) (right), Copyright © 2021 Published by Elsevier B.V. [17]

the electron mobility of ETL but still there is big, unbalanced charge issue which causes the low device performance to reduce the electron mobility of Mg-doped ZnO ETL. In 2020, Wei et al. investigated the ZnMgO doped with Cl [22]. Interestingly, Cl doping upshifts the energy level, resulting in a better charge balance between the EML and ETL. Wei claimed that Cl doping not only reduced charge transport, but also reduced exciton quenching and provided a charge balance for recombination in the emitting layer. A maximum EQE of 4.0% was reported for typical (DMA)<sub>3</sub>P-based InP QLEDs (Fig. 3b), and they claimed that it was the maximum reported to date. The limitations of using doped materials still exist and Ali et al. utilized some antibiotic materials to control the charge balance of Cd-free QLEDs through controlling the ETL [17]. They doped a ZnO-based ETL with ampicillin and realized that the formation of an interfacial dipole balanced the charge by aligning the energy bands. They controlled the polarity of ampicillin by controlling the pH of the ampicillin-based ETL. Through the variation in the pH of the charge transportation layers in ZnO-based ETL, ampicillin acted as an anion around pH 7.5 and created a weak interfacial dipole, lowering the conductivity of the ETL. A maximum EQE of 4.70% has been reported for typical (DMA)<sub>3</sub>P-based InP QLEDs, as shown in Fig. 3c.

## Recent Progress in HTL

Generally, the charge balance required to achieve a high device performance was achieved by modifying the ETL. Another desirable approach to achieve better charge balance is to modify the HIL/HTL [69–71]. Different techniques have been used to modify the HIL/HTL, such as using multilayer HTLs, doping with other materials to improve conductivity, or adding dipole layers between the EML and HTL to achieve better energy levels [72]. Kim et al. used F4-TCNQ, 2,3,4,6-tetrafluoro-7,7,8,8-tetracyanoquinodimethane as the p-type dopant material and diffused it between the HIL and HTL through thermal; annealing this p-type dopant improved the charge balance and enhanced the hole injection efficiency, resulting in an improvement in the EQE of Cd-free QLEDs from 1.6 to 3.78% [73]. Ali et al. used HIL doping to improve the charge balance, resulting in an increase in the EQE of QLEDs [17]. They found that the usage of ampicillin with HIL creates a strong interfacial dipole ( $J$ -aggregation) which reduced the HOMO levels and increased the conductivity of PEDOT:PSS. This reduction in energy barrier between the HIL/EML and ETL improved the charge balance and enhanced the device performance EQE of 4.7% as shown in Fig. 4a. Similarly, Zhong et al.

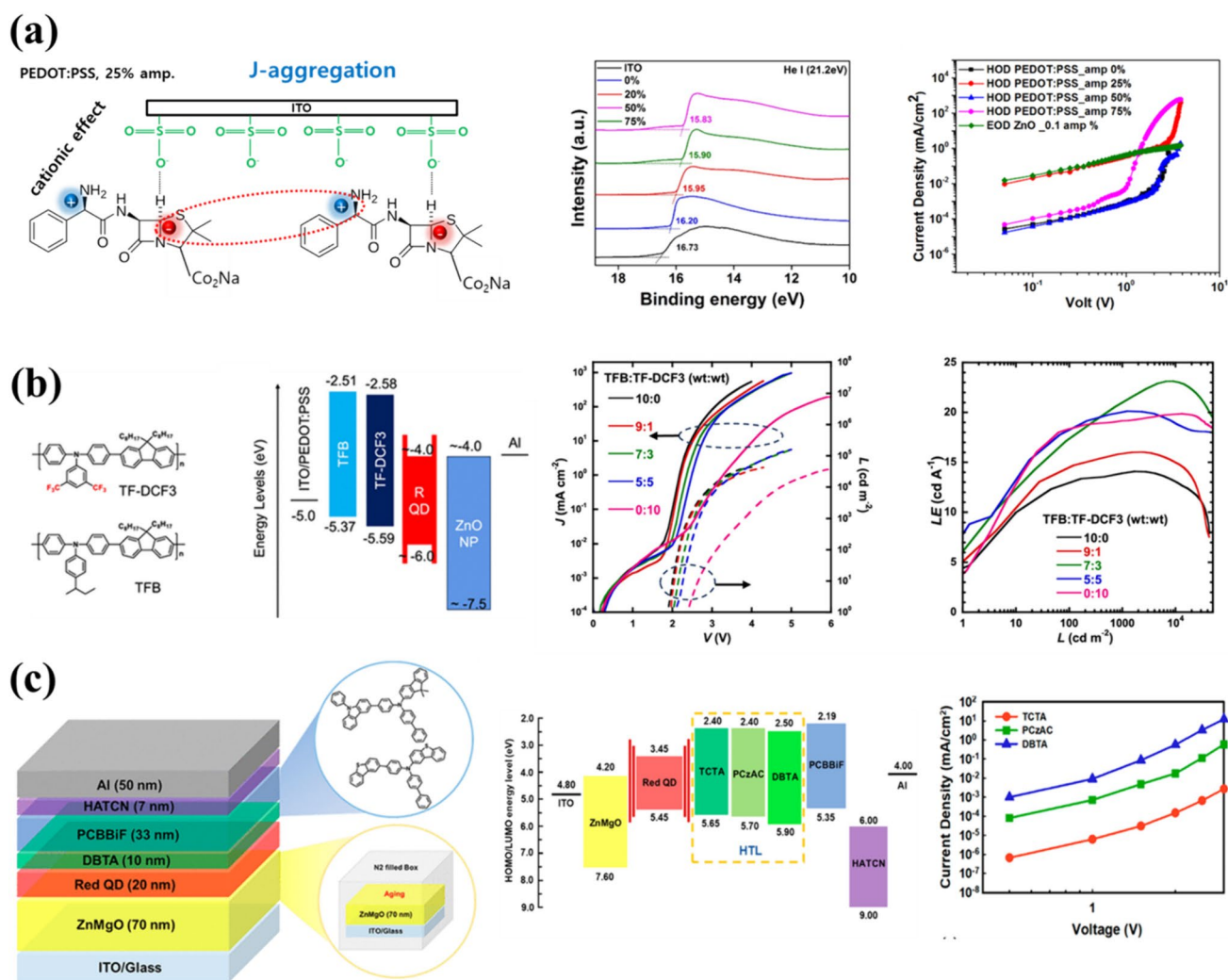


**Fig. 4** **a** Schematic ampicillin and PEDOT:PSS chemical interaction (left), energy level and  $J$ - $V$  characteristics of different HODs (based on different HTL) (right), Copyright © 2021 Published by Elsevier B.V., **b** schematic of TF-DCF<sub>3</sub> and TFB with energy level diagram (left),  $J$ - $V$  characteristics of different HODs (based on different HTL)

(right), Copyright © 2023, American Chemical Society and **c** schematic of QLED with different HTLs (left), energy level and  $J$ - $V$  characteristics of different HODs (based on different HTL) (right) CC BY-NC 3.0 DEED

modified an HTL using two conjugated polymers, TFB and TF-DCF<sub>3</sub>, to modify the surface energy, energy levels, and hole transport mobility [74], as shown in Fig. 4b. Yeom et al. suggested that the difference between the electron and hole mobilities of the ETL and HTL caused charge imbalance and exciton quenching [75]. To overcome this issue, they designed a new HTL material, DBTA (*N*-([1,1'-biphenyl]-4-yl)-*N*-(4-(dibenzo-thiophen-2-yl)phenyl)dibenzo[*b,d*]thiophen-2-amine), with deep highest occupied molecular orbital (HOMO) and high hole mobility. The red InP-based QLED, designed with an inverted structure, achieves a current efficiency of 23.4 cd/A, a lifespan of 72,848 h at an illumination of 100 cd/m<sup>2</sup>, and an external quantum efficiency (EQE) of 21.8%. This EQE is the highest value recorded for red InP QLEDs, as shown in Fig. 4c. Non-radiative

recombination centers can be generated at the interface of organic hole injection/transport materials. The development of p-type inorganic materials was proposed to overcome the lifespan issue of QD-LED. A hydrophilic NiO material with deep HOMO level could be a better replacement for inorganic HTL [76]. Other doped inorganic HTL were also reported to be Cl-passivated tungsten phosphate (Cl-TPA), which was reported by Cao et al. [77] and displayed enhanced carrier concentration, which improved the EQE and lifespan, Fe-doped inorganic HTL reported by Zhang et al. [78], which improved its stability and EQE, and a Mg-doped inorganic HTL was reported by Jiang et al. [79]. Different organic and inorganic HIL/HTL reported are listed in Table 1. QLEDs, while known for their excellent color reproduction and brightness, struggle with achieving the

**Table 1** QD-LED performance based on different HIL/HTL

|           | (HIL)/HTL   | HOMO (eV) | EQE (%) | max. lum (cd/m <sup>2</sup> ) | Lifetime    | Year | ref  |
|-----------|---|-----------|---------|-------------------------------|-------------|------|------|
| Organic   | PEDOT/TFB   | 5.30      | 4.70    | 2445                          |             | 2022 | [17] |
|           | PEDOT/cross-link-TFB  |           | 8.9     | 119 600                       |             | 2017 | [77] |
|           | PEDOT/TC-PDA-CBP  | 5.68      | 8.2     | 23 895                        | 19.5 h      | 2020 | [78] |
|           | PEDOT/PVK/TPD, TCTA, CBP  | 5.8       | 6.5     | 23,900                        |             | 2013 | [79] |
|           | PEDOT/PVK/TFB   | 22.1      |         | 98,000                        |             | 2018 | [80] |
|           | PEDOT/PVK/TPD   |           | 13.4    | 45 310                        |             | 2018 | [81] |
|           | PEDOT/PVK:OXD-7   | 6.5       | 0.32    | 1672                          |             | 2020 | [82] |
|           | PEDOT/TFB:CBP   |           | 30.0    | 963,433                       |             | 2022 | [83] |
|           | PEDOT/PF8Cz   | 5.4       | 28.7    | 200,000                       | 2 570 000 h | 2022 | [84] |
| Inorganic | NiO   | 6.7       | 0.18    |                               |             | 2006 | [73] |
|           | NiO/p-TPD   |           | 2.45    | 1000                          |             | 2014 | [85] |
|           | NiO/Al <sub>2</sub> O <sub>3</sub>                                    |           | 20.5    | 20,000                        |             | 2017 | [86] |
|           | NiMgO/MgO   | 9.1       | 1.5     | 4000                          | 24,724      | 2019 | [76] |
|           | Fe-NiO/TFB  | 5.7–6.5   | 3.8     | 27,624                        | 11,490      | 2020 | [75] |
|           | Cl@TPA  | 5.39      | 9.3     | 32,595                        | 104,000     | 2021 | [74] |
|           | V <sub>2</sub> O <sub>5</sub> /PVK                                    |           | 7.3     | 11,908                        | 14,000      | 2017 | [87] |
|           | Cu <sub>2</sub> SnS <sub>3</sub> -Ga <sub>2</sub> O <sub>3</sub> /PVK | 5.4       | 14.9    | 73,820                        |             | 2018 | [88] |

high resolution and precise material placement required for advanced applications [18]. In addition, the traditional deposition methods used in QLEDs fabrication often result in significant material wastage and challenges in integrating components within complex devices. In contrast, patterning-based techniques, such as photolithography and nanoimprinting, offer superior control over material placement, enabling the creation of intricate device architectures with enhanced performance and reliability [89]. These methods also improve material efficiency, reduce production costs, and support scalable manufacturing processes. As a result, the transition to patterning-based devices opens up new possibilities for innovation in microelectronics, advanced display technologies, and other high-tech applications.

## Techniques of Quantum Dot Patterning

Previous research on EML, ETL, and HTL has been conducted to achieve high efficiency in QLEDs. However, for the realization of next-generation displays, where R/G/B subpixels form a main pixel and miniaturization is essential, advanced patterning technologies are required. These technologies are crucial because during the conventional photolithography, QDs thin films are often exposed to various chemical solvents and can sustain significant damage, thereby failing to maintain their pre-patterning efficiency. Research on quantum dot patterning, which both advances patterning techniques and preserves efficiency, has been actively pursued, employing a variety of methods including coating and patterning with stability PR, direct patterning

of QD thin films, patterning through inkjet printing, and transfer printing techniques.

## Photoresist-Based Patterning for Quantum Dot Applications

In the realm of quantum dots patterning, photolithography is a widely adopted technique for pattern formation, owing to its capability to generate high-resolution patterns using conventional equipment and processes. Nonetheless, when quantum dots are synthesized via solution processes, complications emerge because of the presence of organic ligands that envelope their surfaces. These ligands pose challenges in coating quantum dots with polar solvents, such as PR, thereby increasing the risk of quantum dot damage from the solvents, developers, and resist removal agents utilized during the process [31, 93]. Hence, it is crucial to devise patterning procedures that utilize orthogonal quantum dots and process solvents to mitigate the risk of quantum dot damage.

Ji et al. introduced a quantum dot patterning technique utilizing bottom-up photolithography (Fig. 5a) [94]. This method involves creating sacrificial layer patterns using a PR, followed by material deposition to form patterns, eliminating the need for etching quantum dot films, thereby reducing solvent exposure. AZ5124E PR was employed to fabricate sacrificial layer patterns, with a hexamethyldisilazane (HMDS) coating of the substrate during lift-off to prevent quantum dot detachment, leading to the successful formation of quantum dot pixels. The lithography process was iterated to generate red, green, and blue (R/G/B) pixels with a width

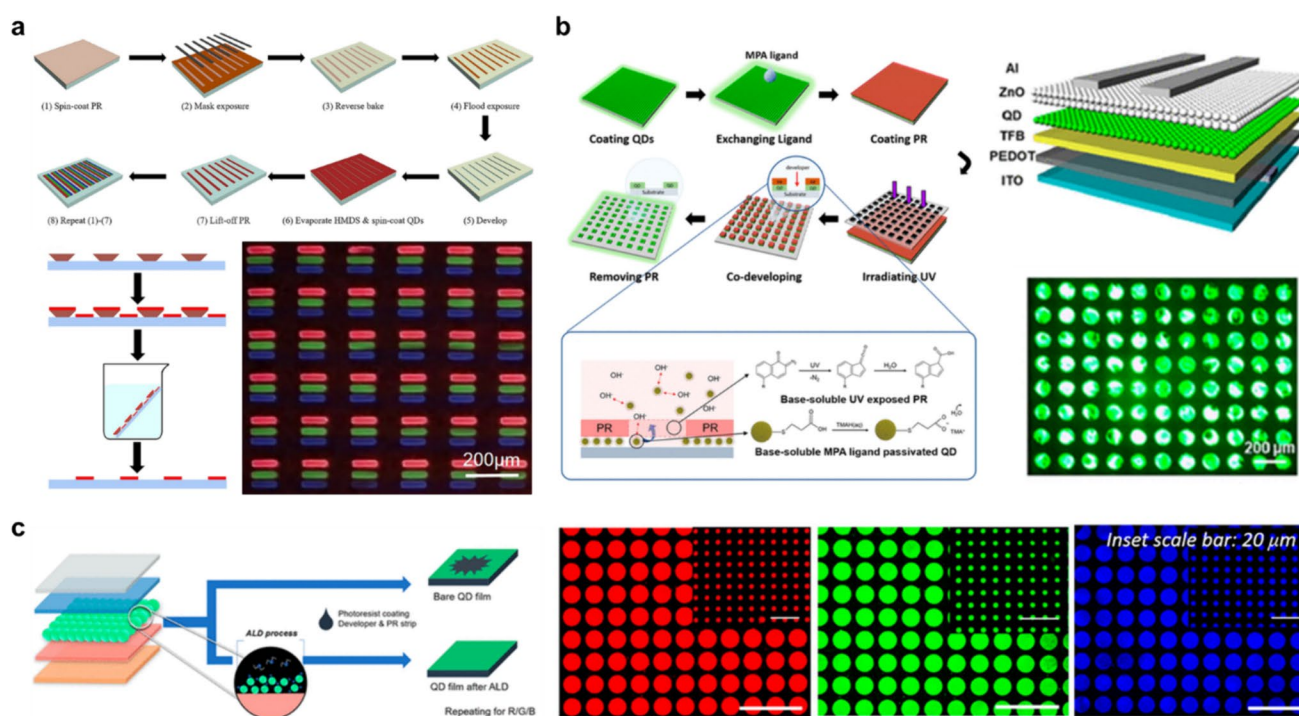


**Fig. 5** Using a PR-based process to shape quantum dot patterns, **a** R/G/B QLED pattern formed using sacrificial layer patterning, Copyright © 2018, Society for Information Display [94], **b** QLED pattern achieved through dual-ligand passivation, Copyright © 2022, Ameri-

can Chemical Society [31], **c** R/G/B QLED pattern stabilized via zinc oxide ALD deposition, Copyright © 2021, American Chemical Society [95]

of 400  $\mu\text{m}$ , confirming the feasibility of quantum dot display implementation via bottom-up lithography.

In a previous study, we developed a photolithography-based patterning technology aimed at minimizing quantum dot degradation from solvents during the process through ligand engineering (Fig. 5b) [31]. The organic ligands on quantum dot surfaces were replaced with dual ligands containing carboxyl and thiol groups. Thiol groups in the dual ligands strongly bind to quantum dot surfaces, preventing solvent-induced degradation during photolithography, whereas carboxyl groups react with alkaline substances in developers, enabling the simultaneous removal of the PR and ligands during development without separate etching processes, thus preventing quantum dot damage by developers. Through this developed photolithography-based quantum dot patterning process, we achieved minimum width, 10  $\mu\text{m}$  quantum dot patterns (approximately 2540 PPI), with QLEDs produced using the patterning process exhibiting similar characteristics to those produced without patterning. In addition, we demonstrate the applicability of our patterning technique to multi-color quantum dot patterning and flexible substrates such as PET, suggesting the potential application of ligand engineering and photolithography-based quantum dot patterning in next-generation high-resolution light-emitting devices.

Kim et al. investigated a quantum dot patterning technology that facilitates high-efficiency QLEDs pattern fabrication by depositing ZnO films on quantum dot surfaces using atomic layer deposition (ALD) (Fig. 5c) [95]. Sequential exposure of diethylzinc (DEZ) and water molecules on quantum dots resulted in ZnO film formation on the quantum dot surfaces, enhancing solvent resistance to organic solvents and enabling direct PR coating on quantum dots for high-resolution patterning via photolithography. Through continuous quantum dot surface ZnO ALD-based photolithography processes, they successfully implemented high-resolution 3-color pattern films (800 PPI), including primary colors R/G/B and multi-color QLEDs.

### Direct Photopatterning

Direct photopatterning, which proceeds with lithography without PR, has garnered attention for preventing quantum dot damage caused by solvents included PR during the lithography processes. Direct photopatterning allows the formation of high-resolution patterns with fewer process steps, making it easily applicable to existing display manufacturing processes [96–98]. The development of photosensitive ligands attached to QD surfaces is essential for direct photopatterning. Many researchers have studied



various crosslinking molecules that form organic and inorganic ligands.

One of the most seminal papers in the field of quantum dots direct patterning, Wang et al. addressed these challenges by developing a patterning method using photosensitive inorganic ligands, termed Direct Optical Lithography of Functional Inorganic Nanomaterials (DOLFIN) [98]. In this study, quantum dots were passivated with ion pairs comprising photoacid generators (PAGs) cations, such as  $\text{Ph}_2\text{I}^+$  or  $\text{Ph}_3\text{S}^+$ , which possess photoreactive ligands and anions that enhance the colloidal stability on the quantum dot surface. The PAG molecules decompose upon photon absorption, releasing acidic cations that react with anions or the quantum dot surface and altering the dissolution rate of quantum dots in those regions. Materials containing anions, such as  $\text{Cs}_2\text{N}_3^-$ , which decompose into  $\text{SCN}^-$  ions and  $\text{N}_2$ , and S upon photon absorption, can also be used as photoreactive ligands. Quantum dots with inorganic ligands dissolve easily in polar solvents such as DMF or DMSO, whereas those with altered solubility owing to the photodegradation of photoreactive ligands do not dissolve in these solvents, allowing the selective removal of unexposed quantum dots to form patterns. Various wavelengths ranging from ultraviolet to visible light can be utilized for direct photopatterning by varying the PAG material used in DOLFIN. Successful implementation of  $10\ \mu\text{m}$ -width quantum dot linear patterns using DOLFIN demonstrated that the optical and electrical properties of quantum dot pixels formed through patterning remained similar to those of unpatterning quantum dots, proving the feasibility of high-resolution patterning without compromising quantum dot characteristics. The research

group further analyzed the ligands applicable to DOLFIN in subsequent studies to develop optimized ligand systems for various wavelengths. In addition, they successfully developed the Direct Electron-Beam Lithography of Functional Inorganic Nanomaterials (DELFIN) using E-beam, achieving high-resolution quantum dot patterns with line widths of  $30\ \text{nm}$  [99].

Kim et al. discussed direct photopatterning technology by adding photo-crosslinking agents to quantum dot solutions (Fig. 6a) [100]. In this study, 2,2-bis((14-azido-2,3,5,6-tetrafluorobenzoyloxy) methyl)propane-1,3-diyl bis(4-azido-2,3,5,6-tetrafluorobenzoate) (4Bx) was used as a photo-crosslinking agent, which, with four crosslinking units per molecule, allowed patterning with a minimal amount (within 5 wt%) to prevent the deterioration of the electrical characteristics during the patterning process. 4Bx can function as a photo-crosslinking agent in most materials containing carbon-hydrogen chains, making it applicable to the fabrication of patterns in organic ligands, including quantum dots.

Yang et al. presented a solution-based processing technique for creating quantum dot patterns using the light-induced ligand crosslinker, ethane-1,2-diyl bis(4-azido-2,3,5,6-tetrafluorobenzoate) (Fig. 6b) [97]. This crosslinker, featuring two azide end groups, can bind to neighboring quantum dot ligands upon UV exposure to form durable quantum dot films. Various CdSe-based core-shell QDs of different colors can be patterned photochemically by leveraging this light-induced crosslinking process. They demonstrate patterns of red, green, and blue primary colors with sub-pixel dimensions of  $4\ \mu\text{m} \times 16\ \mu\text{m}$ , achieving a

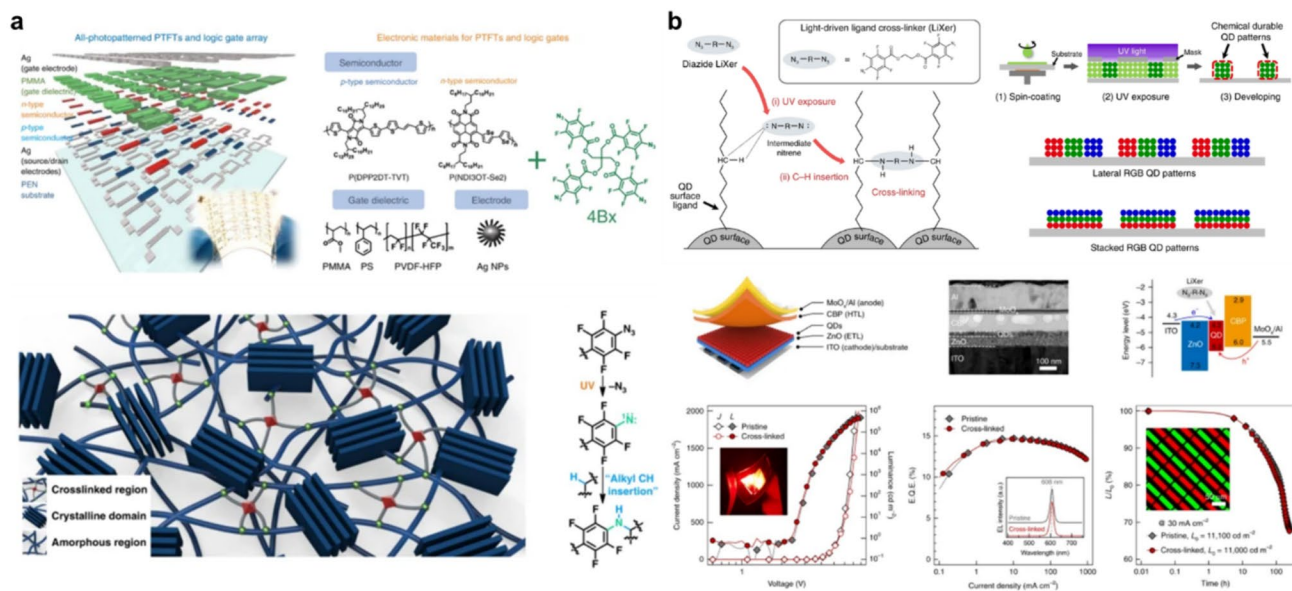


**Fig. 6** Applying direct photopatterning technology to shape quantum dot patterns, **a** nano-patterning based on photo-crosslinkable material 4Bx, Copyright © 2020, Springer Nature [100], **b** patterned QLED achieved via dual organic ligands, Copyright © 2020, Springer Nature [97]

resolution exceeding 1400 pixels per inch. Importantly, this process is non-destructive, preserving the photoluminescence and electroluminescence properties of quantum dot films after crosslinking. Furthermore, they showcase red-crosslinked QD light-emitting diodes with an impressive external quantum efficiency of up to 14.6%.

Hahm et al. devised a dual organic ligand-based direct photopatterning method to mitigate quantum dot degradation caused by byproducts, such as acidic substances, during the decomposition of inorganic ligands [101]. This dual organic ligand consists of photo-crosslinkable ligands (PXL) and dispersing ligands (DL), where PXL enables patterning by forming covalent bonds with adjacent ligands upon exposure to ultraviolet light. To meet the patterning requirements, PXL accounts for less than 10 mol% of the total ligands, whereas DL, comprising over 90 mol%, can be varied to disperse the QDs in solvents with different solubilities. By leveraging the excellent photo-crosslinking properties of organic ligands and the freedom to disperse in different solvents, they successfully dispersed quantum dots of different colors in solvents with varying solubilities

to achieve a high-resolution R/G/B pattern of 15,875 PPI. In addition, the production of QLED confirmed that the photo-crosslinking phenomenon of PXL did not impede the charge transport capability of the quantum dots, unlike previous photo-crosslinkable ligands.

## Inkjet Printing

Unlike photolithography, the technology for forming patterns using inkjet printing requires simple processes without the need for complex procedures, making it a promising next-generation QD patterning technique because of its ability to use QD ink synthesized through solution processes [102]. However, conventional inkjet printers have limitations in terms of pattern resolution, typically in the range of tens of micrometers, owing to the size constraints of the ejected droplets. Various studies are currently underway to overcome this limitation.

Han et al. addressed the resolution limitations of inkjet printing by employing aerosol jet printing to form quantum dot pixels (Fig. 7a) [103]. The aerosol jet printing technique

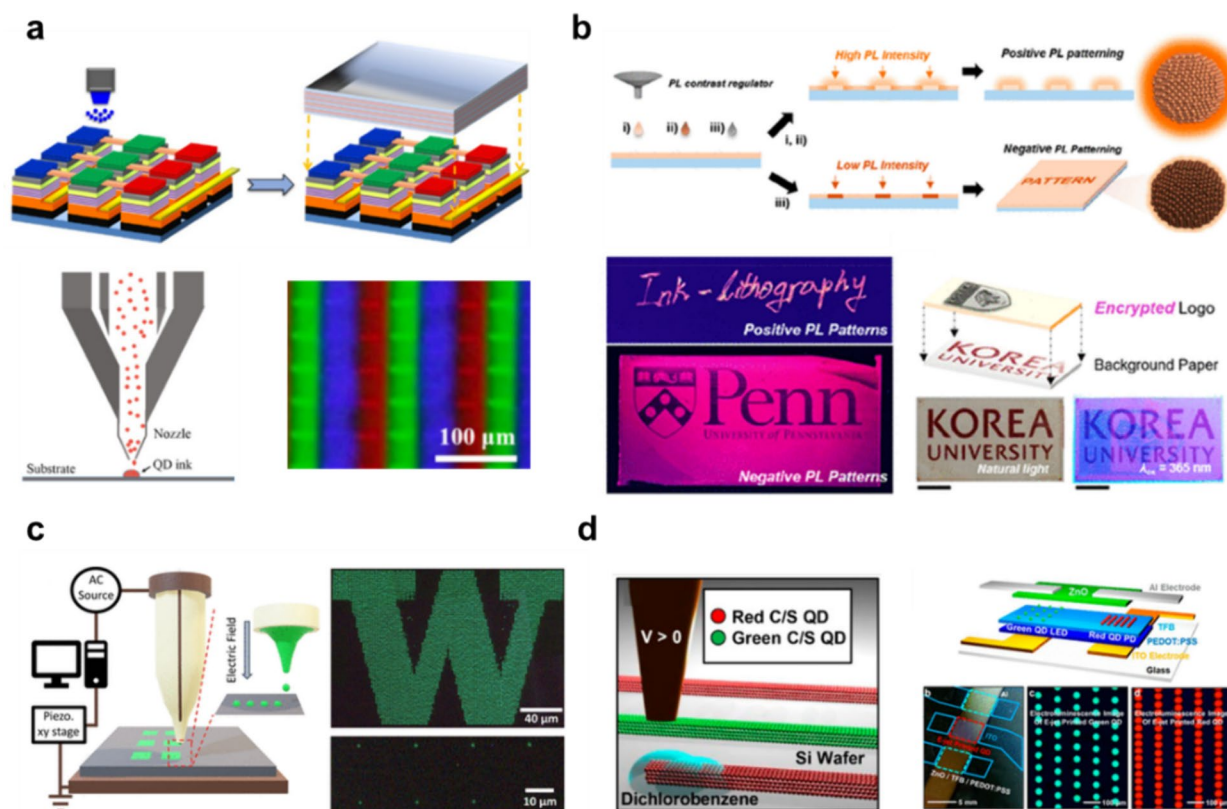


**Fig. 7** Researchers have realized quantum dot patterns through inkjet printing technology as follows: **a** R/G/B-patterned QLEDs based on aerosol jet printing, Copyright © 2015, Optica Publishing Group [103], **b** a quantum dot patterning technique utilizing ink lithography, Copyright © 2021, American Chemical Society [106], **c** an investiga-

tion into high-resolution patterning employing electrohydrodynamic inkjet printing, Copyright © 2022, American Chemical Society [104], and **d** R/G/B-patterned QLEDs fabricated using electrohydrodynamic inkjet printing, Copyright © 2015, American Chemical Society [105]

forms finer patterns by creating a gas flow around the nozzle, which is advantageous for quantum dot pattern formation because of the high viscosity limits of the inks used. This research group successfully produced an R/G/B QLED array with a width of 40  $\mu\text{m}$  (approximately 635 PPI) by forming quantum dot pixel patterns on a micro-UV LED pixel array, demonstrating the potential for high-resolution display fabrication using inkjet printing.

Cohen et al. developed a high-resolution perovskite QD patterning technology that overcomes the limitations of conventional inkjet printing using electrohydrodynamic (EHD) inkjet printing (Fig. 7b) [104]. The minimum droplet size generated from printer nozzles is limited by the droplet surface energy and viscosity. EHD inkjet printing applies an electric field to printer nozzles to overcome these limitations, enabling the creation of smaller droplets. In this research, they successfully formed perovskite quantum dot patterns with a minimum diameter of 200 nm and a minimum width of 2  $\mu\text{m}$  (approximately 12,700 PPI) through EHD inkjet printing, confirming the maintenance of quantum dot characteristics after patterning.

Kim et al. from the University of Illinois optimized the operating conditions of EHD inkjet printing to produce high-resolution quantum dot patterns and implemented QLEDs based on them (Fig. 7c) [105]. They managed printing conditions such as nozzle hole size and voltage to effectively form various shapes of ultrafine patterns, including circular patterns with a diameter of 3.9  $\mu\text{m}$  and linear patterns with a width of 250  $\mu\text{m}$ . They also illustrated the implementation of single-color and multi-color QLED arrays, indicating that the EHD inkjet printing technology could be a powerful tool for high-resolution display fabrication.

In our previous study, Ahn et al. investigated an ink lithography technique using inkjet printing by substituting ligands of quantum dot films to selectively alter the solubility (Fig. 7-d) [106]. Parameters such as ink viscosity and surface tension must be within certain ranges to fabricate high-resolution patterns using inkjet printing. In this study, a solution of 0.5 v/v% ethylene glycol (EG)/IPA was prepared to dissolve various ligands while ensuring precise pattern formation. Through ink lithography, we demonstrated the performance of QD-based devices, such as sensors and transistors, by simultaneously forming QD patterns and ligand substitutions, thereby proving the feasibility of using inkjet printing to fabricate QD-based devices.

## Transfer Printing

Transfer printing is a technique used for forming quantum dot patterns using a substrate on which the patterns are formed during the transfer process. This method does not use solvents during the process, eliminating the risk of quantum dot damage due to chemical exposure and favoring

large-area pixel fabrication. Typically, in transfer printing, a patterned elastomeric stamp is used to transfer quantum dots; however, as the pixel size decreases, cracks may occur in the transferred quantum dot film, preventing complete transfer [107, 108].

To solve this problem, Choi et al. engineered an etching-transfer printing technique to implement intact high-resolution quantum dot pixels proficiently (Fig. 8a) [109]. Initially, using finite element analysis, they analyzed the causes of cracks in the quantum dot film during the transfer process. The stress concentrates on the quantum dot film located at the edges of the pattern during the elastomeric substrate contacting and detaching, propagating cracks from that point and compromising the resolution of the quantum dot pattern. In this study, quantum dots coated on a donor substrate were transferred to a substrate with etched patterns, and quantum dot patterns remaining on polydimethylsiloxane (PDMS) were transferred to the target substrate, forming quantum dot patterns. Etching transfer printing utilized a flat PDMS substrate structure, distributing stress evenly, and resulted in intact high-resolution R/G/B quantum dot patterns with a minimum pixel size of 6  $\mu\text{m}$  (2460 PPI). Furthermore, through repetitive patterning processes, they successfully fabricated red/green/blue QLED patterns and white LED (WLED), thereby proving the feasibility of high-resolution QD-based display fabrication via transfer printing.

Although transfer printing offers excellent optical properties by avoiding solvent use, maintaining the performance of solvent-sensitive materials such as perovskites while achieving high-resolution patterns is challenging [110–112]. However, owing to the weak inter-dot interactions in perovskite quantum dots, internal cracks easily occur during the film transfer process, posing difficulties in forming perovskite quantum dot pixels via transfer printing.

Kwon et al. explored an etching-transfer printing technique combined with organic charge transport layer deposition to prevent internal cracking in perovskite quantum dot films during transfer (Fig. 8b) [113]. The cause of crack formation in the perovskite films during transfer is attributed to the weaker van der Waals forces between the perovskite quantum dots compared to the van der Waals forces acting between the perovskite quantum dots/PDMS stamp. In this study, they enhanced the interactions between perovskite quantum dots by replacing surface ligands with shorter ligands and reduced the adhesion between 2,2',2''-(1,3,5-benzinetriyl)-tris(1-phenyl-1-H-benzimidazole) (TPBi)/PDMS stamp by depositing an organic electron transport layer like TPBi, thereby preventing cracks during the transfer process. They successfully fabricated R/G/B pixels with a minimum size of 3  $\mu\text{m}$  (2550 PPI) by utilizing crack-preventing transfer processes. Moreover, high-density perovskite quantum dot films were formed owing to the pressure during the transfer process, and they implemented

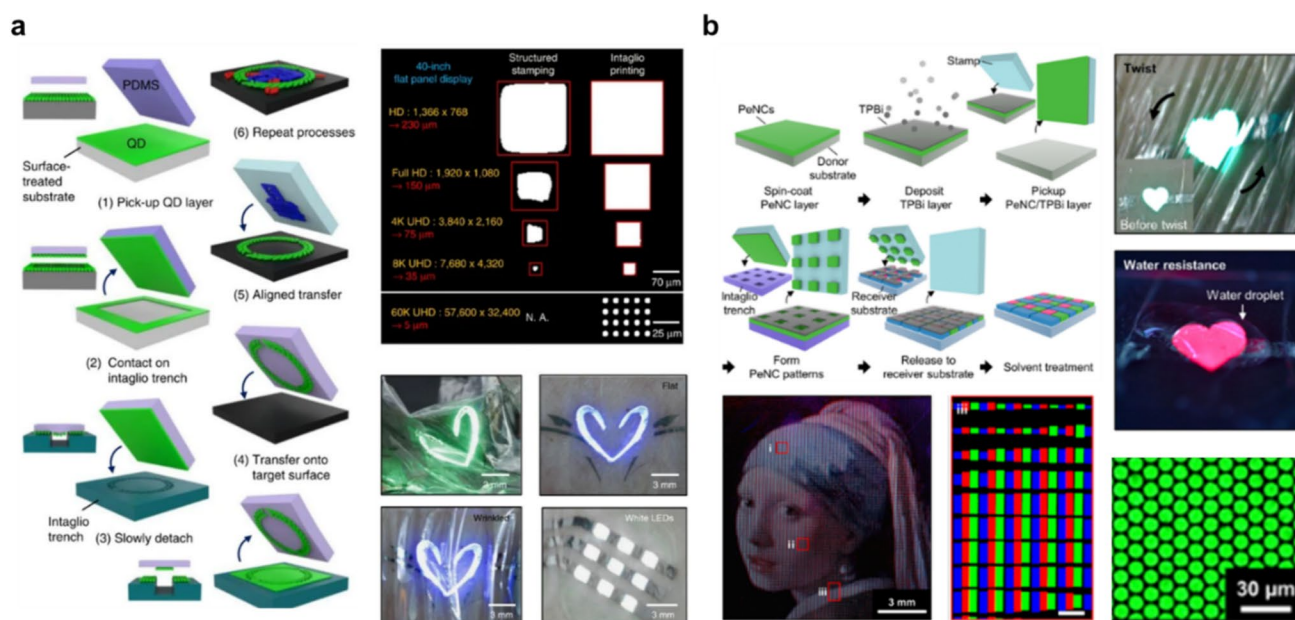


**Fig. 8** For quantum dot patterning, the following techniques based on quantum dot transfer technology have been employed: **a** Uniform R/G/B QLED patterns achieved through nanoimprint lithography, Copyright © 2015, Springer Nature [109], **b** research on full-color

QLED patterning using charge transport layer insertion in the transfer process for perovskite, Copyright 2022, The American Association for the Advancement of Science [113]

high-efficiency QD-LEDs, demonstrating the advantages of display fabrication via transfer printing.

### Patterned Quantum Dots Light-Emitting Diodes

The modification of ETL and HTL materials, along with advanced patterning technologies, aims to ultimately fabricate and commercialize quantum dot-based electroluminescent display panels. Patterning processes, whether physical or chemical, are employed to pattern quantum dots (QDs), thereby preventing damage to QDs during the QLED fabrication process. The performance of QLEDs fabricated using various patterning processes is presented in Table 2. In our previous study, we utilized a dual-ligand approach to prevent the PR components from attacking QDs. The patterned QLEDs achieved a luminance of 23,500 cd/m<sup>2</sup> and an external quantum efficiency (EQE) of 2.95%, with a pattern size of less than 100 μm [31]. Without the use of PR, QLEDs directly patterned by mixing a photosensitizer within the QD

compound achieved a luminance of over 100,000 cd/m<sup>2</sup> and an EQE of over 20% and demonstrated a 10 × 10 array with R/G/B patterns [101]. In addition, QLEDs patterned using inkjet and transfer printing methods exhibited a luminance of over 36,000 cd/m<sup>2</sup> and an EQE of over 2.5%, with a pattern size of less than 50 μm [105, 109].

### Summary

Researchers have shifted their focus to the commercialization of EL-based luminance devices since the commercialization of PL-based luminance devices. Although EL-based devices have reached their theoretical performance limit, there remains a need for performance improvement. For this purpose, both the ZnO-based electron transport layer and hole transport layer require enhancements to align the energy levels. Compared to other electroluminescent devices, QLEDs offer the advantage of easier implementation of

**Table 2** QD-LED performance based on various quantum dots patterning techniques

| Patterning techniques | Compositions (core/shell/shell)  | Luminance (cd/m <sup>2</sup> ) | EQE (%) | Pattern size (μm) | Ref   |
|-----------------------|--|--------------------------------|---------|-------------------|-------|
| Photoresist-based     | CdSe/ZnS   | 23,500                         | 2.95    | 100 μm            | [31]  |
| Direct                | CdSe/Cd <sub>x</sub> Zn <sub>1-x</sub> Se/ZnSe <sub>y</sub> S <sub>1-y</sub> | > 100,000                      | > 20    | < 300 μm          | [101] |
| Inkjet                | CdSe/ZnS   | 36,000                         | 2.5     | 50 μm             | [105] |
| Transfer print        | CdSe/ZnS   | 14,000                         | 2.35    | 150 μm            | [109] |

high-resolution patterning due to their solution processability. Extensive research efforts aimed at preventing the degradation of QD characteristics due to physical and chemical reactions during printing and patterning processes have significantly advanced QD-based displays. These advancements have not only optimized the fabrication process but also paved the way for the seamless integration of cutting-edge technologies, such as virtual reality (VR), augmented reality (AR), mixed reality (MR), and high-resolution ultra-small area displays. Consequently, these next-generation displays are poised to transform various industries by delivering immersive visual experiences and enhanced functionality, driving innovation and opening new possibilities for applications across diverse fields.

**Acknowledgements** This research was supported by the Basic Science Research Program through the National Research Foundation of Korea (NRF) funded by the Ministry of Science and ICT (NRF-2018M3D1A1059001, NRF-2022R1A2C4001517, RS-2024-00411892, RS-2024-00438059), Materials Innovation Project (NRF-2021M3H4A3026733) and the Ministry of Trade, Industry & Energy (RS-2023-00256247, RS-2024-00433146).

**Data Availability** Data sharing is not applicable to this article as no new data were created or analyzed in this study.

## References

1. T.H. Le, D.H. Lee, J.H. Kim, S.J. Park, Synthesis of enhanced fluorescent graphene quantum dots for catecholamine neurotransmitter sensing. *Korean J. Chem. Eng.* **37**, 1000–1007 (2020)
2. S. Jeon, J. Ahn, M.C. Jung, H.K. Woo, J. Bang, B.K. Jung, S. Oh, S.Y. Lee, K.J. Lee, T. Paik, Defect Engineering of Metal Halide Perovskite Nanocrystals via Spontaneous Diffusion of Ag Nanocrystals, *Small*, (2023) 2307032.
3. S. Jeon, J. Ahn, H. Kim, H.K. Woo, J. Bang, W.S. Lee, D. Kim, M.A. Hossain, S.J. Oh, Investigation of the chemical effect of solvent during ligand exchange on nanocrystal thin films for wearable sensor applications. *J. Phys. Chem. C* **123**, 11001–11010 (2019)
4. S. Won, J. Kim, The detection of Fe (III) and ascorbic acid by fluorescence quenching and recovery of carbon dots prepared from coffee waste. *Korean J. Chem. Eng.* **39**, 2826–2833 (2022)
5. W.S. Lee, Y.G. Kang, H.K. Woo, J. Ahn, H. Kim, D. Kim, S. Jeon, M.J. Han, J.-H. Choi, S.J. Oh, Designing high-performance CdSe nanocrystal thin-film transistors based on solution process of simultaneous ligand exchange, trap passivation, and doping. *Chem. Mater.* **31**, 9389–9399 (2019)
6. S. Park, M.-K. Son, S.-K. Kim, M.-S. Jeong, K. Prabakar, H.-J. Kim, The effects of electrolyte additives on the cell performances of CdS/CdSe quantum dot sensitized solar cells. *Korean J. Chem. Eng.* **30**, 2088–2092 (2013)
7. H.K. Woo, H. Kim, S. Jeon, W.S. Lee, J. Ahn, J. Bang, M.S. Kang, S.J. Oh, One-step chemical treatment to design an ideal nanospacer structure for a highly sensitive and transparent pressure sensor. *J. Mater. Chem. C* **7**, 5059–5066 (2019)
8. W.S. Lee, S. Jeon, S.J. Oh, Wearable sensors based on colloidal nanocrystals. *Nano Convergence* **6**, 1–13 (2019)
9. J. Ahn, S. Jeon, W.S. Lee, H.K. Woo, D. Kim, J. Bang, S.J. Oh, Chemical effect of halide ligands on the electromechanical properties of Ag nanocrystal thin films for wearable sensors. *J. Phys. Chem. C* **123**, 18087–18094 (2019)
10. B.K. Jung, S. Jeon, H.K. Woo, T. Park, J. Ahn, J. Bang, S.Y. Lee, Y.M. Lee, S.J. Oh, Janus-like jagged structure with nanocrystals for self-sorting wearable tactile sensor. *ACS Appl. Mater. Interfaces* **13**, 6394–6403 (2021)
11. T. Park, H.K. Woo, B.K. Jung, B. Park, J. Bang, W. Kim, S. Jeon, J. Ahn, Y. Lee, Y.M. Lee, Noninterference wearable strain sensor: near-zero temperature coefficient of resistance nanoparticle arrays with thermal expansion and transport engineering. *ACS Nano* **15**, 8120–8129 (2021)
12. W.S. Lee, D. Kim, B. Park, H. Joh, H.K. Woo, Y.K. Hong, T.I. Kim, D.H. Ha, S.J. Oh, Multiaxial and transparent strain sensors based on synergetically reinforced and orthogonally cracked hetero-nanocrystal solids, *Advanced Functional Materials*, **29** (2019) 1806714.
13. S. Jeon, M.-C. Jung, J. Ahn, H.K. Woo, J. Bang, D. Kim, S.Y. Lee, H.Y. Woo, J. Jeon, M.J. Han, Post-synthetic oriented attachment of CsPbBr<sub>3</sub> perovskite nanocrystal building blocks: from first principle calculation to experimental demonstration of size and dimensionality (0D/1D/2D). *Nanoscale Horizons* **5**, 960–970 (2020)
14. B.K. Jung, H.K. Woo, C. Shin, T. Park, N. Li, K.J. Lee, W. Kim, J.H. Bae, J.P. Ahn, T.N. Ng, Suppressing the dark current in quantum dot infrared photodetectors by controlling carrier statistics. *Adv. Opt. Mater.* **10**, 2101611 (2022)
15. J. Ahn, B.K. Jung, W. Kim, Y.M. Lee, J. Bang, S.Y. Lee, T. Park, Y.K. Choi, J.H. Bae, S.J. Oh, Anchoring Cs<sub>4</sub>PbBr<sub>6</sub> Crystals to PbSe nanocrystals for the fabrication of UV/VIS/NIR photodetectors using halide surface chemistry. *Adv. Opt. Mater.* **11**, 2201833 (2023)
16. Y.K. Choi, T.H. Kim, B.K. Jung, T. Park, Y.M. Lee, S. Oh, H.J. Choi, J. Park, S.I. Bae, Y. Lee, High-Performance Self-Powered Quantum Dot Infrared Photodetector with Azide Ion Solution Treated Electron Transport Layer, *Small*, (2023) 2308375.
17. A. Ali, W. Jiang, Y. Choi, E. Jeon, H. Chae, Enhanced charge balance with antibiotics in both electron and hole transport layers of InP/ZnSexS1-x/ZnS-based quantum dot light-emitting diodes. *J. Alloy. Compd.* **900**, 163449 (2022)
18. J. Kim, J. Roh, M. Park, C. Lee, Recent Advances and Challenges of Colloidal Quantum Dot Light-Emitting Diodes for Display Applications, *Advanced Materials*, (2023) 2212220.
19. S.-Y. Yoon, J.-H. Kim, K.-H. Kim, C.-Y. Han, J.-H. Jo, D.-Y. Jo, S. Hong, J.Y. Hwang, Y.R. Do, H. Yang, High-efficiency blue and white electroluminescent devices based on non-Cd I–III–VI quantum dots. *Nano Energy* **63**, 103869 (2019)
20. W.K. Bae, J. Lim, Nanostructured colloidal quantum dots for efficient electroluminescence devices. *Korean J. Chem. Eng.* **36**, 173–185 (2019)
21. A. Ali, W. Jiang, Y. Choi, B. Kim, K. Lee, H. Chae, Control of the reaction kinetics of monodispersed InP/ZnSeS/ZnS-based quantum dots using organophosphorus compounds for electroluminescent devices. *J. Phys. Chem. Lett.* **14**, 1656–1662 (2023)
22. W. Jiang, H. Chae, Efficiency enhancement of tris (dimethylamino)-phosphine-based red indium phosphide quantum-dot light-emitting diodes via chlorine-doped ZnMgO electron transport layers. *J. Phys. Chem. C* **124**, 25221–25228 (2020)
23. J. Xiong, E.L. Hsiang, Z. He, T. Zhan, S.T. Wu, Augmented reality and virtual reality displays: emerging technologies and future perspectives. *Light Sci. Appl.* **10**, 216 (2021)
24. S.Y. Kim, J.I. Kwon, H.H. Song, G.H. Lee, W.S. Yu, S. Li, M.K. Choi, J. Yang, Effects of the surface ligands of quantum dots on the intaglio transfer printing process. *Appl. Surf. Sci.* **610**, 155579 (2023)
25. S. Y. Bang, Y. -H. Suh, X. -B. Fan, D. -W. Shin, S. Lee, H. W. Choi, T. H. Lee, a J. Yang, S. Zhan, W. H. Chaters, C.

- Samarakoon, L. G. Occhipinti, S. D. Han, S. -M. Jung, and J. M. Kim, Technology progress on quantum dot light-emitting diodes for next-generation displays, *Nanoscale Horiz.* **6**, 68–77, (2021).
26. G. Nedelcu, L. Protesescu, S. Yakunin, M.I. Bodnarchuk, M.J. Grotevent, M.V. Kovalenko, Fast Anion-Exchange in Highly Luminescent Nanocrystals of Cesium Lead Halide Perovskites (CsPbX<sub>3</sub>, X = Cl, Br, I). *Nano Lett.* **15**(8), 5635–5640 (2015)
  27. Q.A. Akkerman, V. D'Innocenzo, S. Accornero, A. Scarpellini, A. Petrozza, M. Prato, L. Manna, Tuning the optical properties of cesium lead halide perovskite nanocrystals by anion exchange reactions. *J. Am. Chem. Soc.* **137**(32), 10276–10281 (2015)
  28. S. Y. Lee, S. Jeon, J. Ahn, J. Bang, H. K. Woo, K. -J. Lee, B. K. Jung, T. Park, D. Son, J. -P. Ahn, and S. J. Oh, Highly stretchable white-light electroluminescent devices with gel-type silica-coated all-inorganic perovskite, *Appl. Surf. Sci.* **563**, 150229, (2021).
  29. Maksym V. Kovalenko, Loredana Protesescu, and Maryna I. Bodnarchuk, Properties and potential optoelectronic applications of lead halide perovskite nanocrystals, *Science* **358** (6364), 745–750, (2017)
  30. L. Protesescu, S. Yakunin, M.I. Bodnarchuk, F. Krieg, R. Caputo, C.H. Hendon, R.X. Yang, A. Walsh, M.V. Kovalenko, Nanocrystals of cesium lead halide perovskites (CsPbX<sub>3</sub>, X = Cl, Br, and I): novel optoelectronic materials showing bright emission with wide color gamut. *Nano Lett.* **15**, 3692–3696 (2015)
  31. J.H. Bae, S. Kim, J. Ahn, C. Shin, B.K. Jung, Y.M. Lee, Y.K. Hong, W. Kim, D.H. Ha, T.N. Ng, J. Kim, S.J. Oh, Direct photolithographic patterning of colloidal quantum dots enabled by UV-crosslinkable and hole-transporting polymer ligands. *ACS Appl. Mater. Interfaces* **14**(42), 47831–47840 (2022)
  32. Z. Cui, D. Yang, S. Qin, Z. Wen, H. He, S. Mei, W. Zhang, G. Xing, C. Liang, R. Guo, Advances, challenges, and perspectives for heavy-metal-free blue-emitting indium phosphide quantum dot light-emitting diodes. *Adv. Opt. Mater.* **11**, 2202036 (2023)
  33. X. Fan, N.E. Stott, J. Zeng, Y. Li, J. Ouyang, L. Chu, W. Song, PEDOT: PSS materials for optoelectronics, thermoelectrics, and flexible and stretchable electronics. *J. Mater. Chem. A* **11**, 18561–18591 (2023)
  34. W. Han, G. Ren, J. Liu, Z. Li, H. Bao, C. Liu, W. Guo, Recent progress of inverted perovskite solar cells with a modified PEDOT: PSS hole transport layer. *ACS Appl. Mater. Interfaces* **12**, 49297–49322 (2020)
  35. Y. Xia, G. Yan, J. Lin, Review on tailoring PEDOT: PSS layer for improved device stability of perovskite solar cells. *Nanomaterials* **11**, 3119 (2021)
  36. Q. Li, S. Cao, P. Yu, M. Ning, K. Xing, Z. Du, B. Zou, J. Zhao, Boosting electroluminescence performance of all solution processed InP based quantum dot light emitting diodes using bilayered inorganic hole injection layers. *Photonics Res.* **10**, 2133–2139 (2022)
  37. G.M. Arumugam, S.K. Karunakaran, C. Liu, C. Zhang, F. Guo, S. Wu, Y. Mai, Inorganic hole transport layers in inverted perovskite solar cells: a review. *Nano Select* **2**, 1081–1116 (2021)
  38. S. Wang, Y. Li, J. Chen, O. Lin, W. Niu, C. Yang, A. Tang, Development and challenges of indium phosphide-based quantum-dot light-emitting diodes, *J. Photochem. Photobiol. C* (2023) 100588.
  39. H.Y. Kim, Y.J. Park, J. Kim, C.J. Han, J. Lee, Y. Kim, T. Greco, C. Ippen, A. Wedel, B.K. Ju, Transparent InP quantum dot light-emitting diodes with ZrO<sub>2</sub> Electron transport layer and indium zinc oxide top electrode. *Adv. Func. Mater.* **26**, 3454–3461 (2016)
  40. J. Guo, C.-J. Zheng, K. Ke, M. Zhang, H.-Y. Yang, J.-W. Zhao, Z.-Y. He, H. Lin, S.-L. Tao, X.-H. Zhang, Novel triazine derivatives with deep LUMO energy levels as the electron-accepting components of exciplexes. *J. Mater. Chem. C* **9**, 939–946 (2021)
  41. J. Yun, J. Kim, B.J. Jung, G. Kim, J. Kwak, Enhanced efficiency and high temperature stability of hybrid quantum dot light-emitting diodes using molybdenum oxide doped hole transport layer. *RSC Adv.* **9**, 16252–16257 (2019)
  42. H. Zhang, S. Chen, X.W. Sun, Efficient red/green/blue tandem quantum-dot light-emitting diodes with external quantum efficiency exceeding 21%. *ACS Nano* **12**, 697–704 (2018)
  43. Z. Wu, P. Liu, W. Zhang, K. Wang, X.W. Sun, Development of InP quantum dot-based light-emitting diodes. *ACS Energy Lett.* **5**, 1095–1106 (2020)
  44. M.L. Steigerwald, A.P. Alivisatos, J. Gibson, T. Harris, R. Kortan, A. Muller, A. Thayer, T. Duncan, D. Douglass, L.E. Brus, Surface derivatization and isolation of semiconductor cluster molecules. *J. Am. Chem. Soc.* **110**, 3046–3050 (1988)
  45. D.J. Suh, O.O. Park, H.-T. Jung, M.H. Kwon, Optical properties and characteristics of the CdSe nanoparticles synthesized at room temperature. *Korean J. Chem. Eng.* **19**, 529–533 (2002)
  46. M.A. Olshavsky, A. Goldstein, A.P. Alivisatos, Organometallic synthesis of gallium-arsenide crystallites, exhibiting quantum confinement. *J. Am. Chem. Soc.* **112**, 9438–9439 (1990)
  47. N. Chestnoy, R. Hull, L. Brus, Higher excited electronic states in clusters of ZnSe, CdSe, and ZnS: Spin-orbit, vibronic, and relaxation phenomena. *J. Chem. Phys.* **85**, 2237–2242 (1986)
  48. O.I. Micic, C.J. Curtis, K.M. Jones, J.R. Sprague, A.J. Nozik, Synthesis and characterization of InP quantum dots. *J. Phys. Chem.* **98**, 4966–4969 (1994)
  49. Y. Wang, A. Suna, W. Mahler, R. Kasowski, PbS in polymers From molecules to bulk solids. *J. Chem. Phys.* **87**, 7315–7322 (1987)
  50. A. Kortan, R. Hull, R.L. Opila, M.G. Bawendi, M.L. Steigerwald, P. Carroll, L.E. Brus, Nucleation and growth of CdSe on ZnS quantum crystallite seeds, and vice versa, in inverse micelle media. *J. Am. Chem. Soc.* **112**, 1327–1332 (1990)
  51. E. Jang, H. Jang, Quantum dot light-emitting diodes. *Chem. Rev.* **123**, 4663–4692 (2023)
  52. T. Fang, T. Wang, X. Li, Y. Dong, S. Bai, J. Song, Perovskite QLED with an external quantum efficiency of over 21% by modulating electronic transport. *Sci. Bull.* **66**, 36–43 (2021)
  53. A.D. Leach, J.E. Macdonald, Optoelectronic properties of CuInS<sub>2</sub> nanocrystals and their origin. *J. Phys. Chem. Lett.* **7**, 572–583 (2016)
  54. T. Uematsu, M. Tepakidareekul, T. Hirano, T. Torimoto, S. Kuwabata, Facile high-yield synthesis of Ag–In–Ga–S quaternary quantum dots and coating with gallium sulfide shells for narrow band-edge emission. *Chem. Mater.* **35**, 1094–1106 (2023)
  55. Y. Kim, S. Ham, H. Jang, J.H. Min, H. Chung, J. Lee, D. Kim, E. Jang, Bright and uniform green light emitting InP/ZnSe/ZnS quantum dots for wide color gamut displays. *ACS Appl. Nano Mater.* **2**, 1496–1504 (2019)
  56. L. Li, P. Reiss, One-pot synthesis of highly luminescent InP/ZnS nanocrystals without precursor injection. *J. Am. Chem. Soc.* **130**, 11588–11589 (2008)
  57. R. Xie, D. Battaglia, X. Peng, Colloidal InP nanocrystals as efficient emitters covering blue to near-infrared. *J. Am. Chem. Soc.* **129**, 15432–15433 (2007)
  58. J. Lim, W.K. Bae, D. Lee, M.K. Nam, J. Jung, C. Lee, K. Char, S. Lee, InP@ ZnSeS<sub>x</sub> core@ composition gradient shell quantum dots with enhanced stability. *Chem. Mater.* **23**, 4459–4463 (2011)
  59. K. Kim, Y.-H. Suh, D. Kim, Y. Choi, E. Bang, B.H. Kim, J. Park, Zinc oxo clusters improve the optoelectronic properties on indium phosphide quantum dots. *Chem. Mater.* **32**, 2795–2802 (2020)
  60. R.F. Ubbink, G. Almeida, H. Iziyi, I. Du Fossé, R. Verkleij, S. Ganapathy, E.R. Van Eck, A.J. Houtepen, A water-free in situ HF treatment for ultrabright InP quantum dots. *Chem. Mater.* **34**, 10093–10103 (2022)

61. F. Chen, P. Lv, X. Li, Z. Deng, F. Teng, A. Tang, Highly-efficient and all-solution-processed red-emitting InP/ZnS-based quantum-dot light-emitting diodes enabled by compositional engineering of electron transport layers. *J. Mater. Chem. C* **7**, 7636–7642 (2019)
62. Y.-H. Won, O. Cho, T. Kim, D.-Y. Chung, T. Kim, H. Chung, H. Jang, J. Lee, D. Kim, E. Jang, Highly efficient and stable InP/ZnSe/ZnS quantum dot light-emitting diodes. *Nature* **575**, 634–638 (2019)
63. C. Liu, C. Xiao, W. Li, Zinc oxide nanoparticles as electron transporting interlayer in organic solar cells. *J. Mater. Chem. C* **9**, 14093–14114 (2021)
64. H.K. Woo, M.S. Kang, T. Park, J. Bang, S. Jeon, W.S. Lee, J. Ahn, G. Cho, D.-K. Ko, Y. Kim, Colloidal-annealing of ZnO nanoparticles to passivate traps and improve charge extraction in colloidal quantum dot solar cells. *Nanoscale* **11**, 17498–17505 (2019)
65. Y. Fu, W. Jiang, D. Kim, W. Lee, H. Chae, Highly efficient and fully solution-processed inverted light-emitting diodes with charge control interlayers. *ACS Appl. Mater. Interfaces* **10**, 17295–17300 (2018)
66. S. Mokarian Zanjani, F. Tintori, S. Sadeghi, P. Linkov, S. Dayneko, A. Shahalizad, H. Pahlevaninezhad, M. Pahlevani, Tailored ZnO Functional Nanomaterials for Solution-Processed Quantum-Dot Light-Emitting Diodes, *Advanced Photonics Research*, 3 (2022) 2200159.
67. H.C. Wang, H. Zhang, H.Y. Chen, H.C. Yeh, M.R. Tseng, R.J. Chung, S. Chen, R.S. Liu, Cadmium-Free InP/ZnSeS/ZnS Heterostructure-Based Quantum Dot Light-Emitting Diodes with a ZnMgO Electron Transport Layer and a Brightness of Over 10 000 cd m<sup>-2</sup>, Small (Weinheim an der Bergstrasse, Germany), 13 (2017).
68. H. Moon, W. Lee, J. Kim, D. Lee, S. Cha, S. Shin, H. Chae, Composition-tailored ZnMgO nanoparticles for electron transport layers of highly efficient and bright InP-based quantum dot light emitting diodes. *Chem. Commun.* **55**, 13299–13302 (2019)
69. T. Davidson-Hall, H. Aziz, Significant enhancement in quantum dot light-emitting device stability via a cascading hole transport layer. *ACS Appl. Mater. Interfaces* **12**, 16782–16791 (2020)
70. H. Chen, K. Ding, L. Fan, W. Liu, R. Zhang, S. Xiang, Q. Zhang, L. Wang, All-solution-processed quantum dot light emitting diodes based on double hole transport layers by hot spin-coating with highly efficient and low turn-on voltage. *ACS Appl. Mater. Interfaces* **10**, 29076–29082 (2018)
71. W. Ji, Y. Lv, P. Jing, H. Zhang, J. Wang, H. Zhang, J. Zhao, Highly efficient and low turn-on voltage quantum dot light-emitting diodes by using a stepwise hole-transport layer. *ACS Appl. Mater. Interfaces* **7**, 15955–15960 (2015)
72. J. Pan, J. Chen, Q. Huang, L. Wang, W. Lei, A highly efficient quantum dot light emitting diode via improving the carrier balance by modulating the hole transport. *RSC Adv.* **7**, 43366–43372 (2017)
73. H. Kim, W. Lee, H. Moon, S.J. Kim, H.K. Chung, H. Chae, Interlayer doping with p-type dopant for charge balance in indium phosphide (InP)-based quantum dot light-emitting diodes. *Opt. Express* **27**, A1287–A1296 (2019)
74. Z. Zhong, H. Quan, J. Zhang, F. Peng, W. Zhong, L. Ying, Improving the performance of quantum dot light-emitting diodes by the enrichment of a fluorinated component on top of a hole transport layer. *ACS Appl. Electron. Mater.* **5**, 6452–6458 (2023)
75. J.E. Yeom, D.H. Shin, R. Lampande, Y.H. Jung, N.N. Mude, J.H. Park, J.H. Kwon, Good charge balanced inverted red InP/ZnSe/ZnS-quantum dot light-emitting diode with new high mobility and deep HOMO level hole transport layer. *ACS Energy Lett.* **5**, 3868–3875 (2020)
76. J.-M. Caruge, J.E. Halpert, V. Bulović, M.G. Bawendi, NiO as an inorganic hole-transporting layer in quantum-dot light-emitting devices. *Nano Lett.* **6**, 2991–2994 (2006)
77. F. Cao, Q. Wu, Y. Sui, S. Wang, Y. Dou, W. Hua, L. Kong, L. Wang, J. Zhang, T. Jiang, All-inorganic quantum dot light-emitting diodes with suppressed luminance quenching enabled by chloride passivated tungsten phosphate hole transport layers. *Small* **17**, 2100030 (2021)
78. Y. Zhang, X. Wang, Y. Chen, Y. Gao, Improved electroluminescence performance of quantum dot light-emitting diodes: a promising hole injection layer of Fe-doped NiO nanocrystals. *Opt. Mater.* **107**, 110158 (2020)
79. Y. Jiang, L. Jiang, F.S. Yan Yeung, P. Xu, S. Chen, H.-S. Kwok, G. Li, All-inorganic quantum-dot light-emitting diodes with reduced exciton quenching by a MgO decorated inorganic hole transport layer, *ACS applied materials & interfaces*, 11 (2019) 11119–11124.
80. Y. Zou, Y. Liu, M. Ban, Q. Huang, T. Sun, Q. Zhang, T. Song, B. Sun, Crosslinked conjugated polymers as hole transport layers in high-performance quantum dot light-emitting diodes. *Nanoscale Horizons* **2**, 156–162 (2017)
81. W. Sun, Y. Deng, Y. Jin, X. Guo, Q. Zhang, Solvent resistant hole-transporting thin films via diacetylene cross-linking and their applications in solution-processed QLEDs. *ACS Appl. Polymer Mater.* **2**, 3274–3281 (2020)
82. M.D. Ho, D. Kim, N. Kim, S.M. Cho, H. Chae, Polymer and small molecule mixture for organic hole transport layers in quantum dot light-emitting diodes. *ACS Appl. Mater. Interfaces* **5**, 12369–12374 (2013)
83. Y. Liu, C. Jiang, C. Song, J. Wang, L. Mu, Z. He, Z. Zhong, Y. Cun, C. Mai, J. Wang, Highly efficient all-solution processed inverted quantum dots based light emitting diodes. *ACS Nano* **12**, 1564–1570 (2018)
84. J. Li, Z. Liang, Q. Su, H. Jin, K. Wang, G. Xu, X. Xu, Small molecule-modified hole transport layer targeting low turn-on-voltage, bright, and efficient full-color quantum dot light emitting diodes. *ACS Appl. Mater. Interfaces* **10**, 3865–3873 (2018)
85. S. Ozguler, H. Diker, S.S. Unluturk, S. Ozelcik, C. Varlikli, Reducing the efficiency roll off and applied potential-induced color shifts in CdSe@ ZnS/ZnS-based light-emitting diodes. *J. Phys. Chem. C* **124**, 14847–14854 (2020)
86. Y. Fang, P. Bai, J. Li, B. Xiao, Y. Wang, Y. Wang, Highly efficient red quantum dot light-emitting diodes by balancing charge injection and transport. *ACS Appl. Mater. Interfaces* **14**, 21263–21269 (2022)
87. Y. Deng, F. Peng, Y. Lu, X. Zhu, W. Jin, J. Qiu, J. Dong, Y. Hao, D. Di, Y. Gao, Solution-processed green and blue quantum-dot light-emitting diodes with eliminated charge leakage. *Nat. Photonics* **16**, 505–511 (2022)
88. H.T. Nguyen, H. Jeong, J.-Y. Park, Y. Ahn, S. Lee, Charge transport in light emitting devices based on colloidal quantum dots and a solution-processed nickel oxide layer. *ACS Appl. Mater. Interfaces* **6**, 7286–7291 (2014)
89. F. Tian, Y. Zhu, Z. Xu, B. Li, X. Zheng, Z. Ni, H. Hu, Y. Chen, J. Zhuang, L. Wu, Achieving highly efficient and stable quantum dot light-emitting diodes with interface modification. *IEEE Electron Device Lett.* **41**, 1384–1387 (2020)
90. W. Ji, S. Liu, H. Zhang, R. Wang, W. Xie, H. Zhang, Ultrasonic spray processed, highly efficient all-inorganic quantum-dot light-emitting diodes. *ACS Photonics* **4**, 1271–1278 (2017)
91. H. Zhang, S. Wang, X. Sun, S. Chen, Solution-processed vanadium oxide as an efficient hole injection layer for quantum-dot light-emitting diodes. *J. Mater. Chem. C* **5**, 817–823 (2017)
92. J. Kim, H.M. Kim, S. Cho, C. Avis, J. Jang, High hall mobility P-type Cu<sub>2</sub>SnS<sub>3</sub>-Ga<sub>2</sub>O<sub>3</sub> with a high work function. *Adv. Func. Mater.* **28**, 1802941 (2018)

93. S. Jeon, S. Y. Lee, S.-K. Kim, W. Kim, T. Park, J. Bang, J. Ahn, H. K. Woo, J.-Y. Chae, T. Park, T.-Y. Seong, and S. J. Oh, All-Solution Processed Multicolor Patterning Technique of Perovskite Nanocrystal for Color Pixel Array and Flexible Optoelectronic Devices, *Adv. Opt. Mater.* **(8)**, 2000501, (2020).
94. T. Ji, S. Jin, H. Zhang, S. Chen, X.W. Sun, Full color quantum dot light-emitting diodes patterned by photolithography technology. *J. Soc. Inf. Disp.* **26**(3), 121–127 (2018)
95. G.-H. Kim, J. Lee, J.Y. Lee, J. Han, Y. Choi, C.J. Kang, K.-B. Kim, W. Lee, J. Lim, S.-Y. Cho, High-resolution colloidal quantum dot film photolithography via atomic layer deposition of ZnO. *ACS Appl. Mater. Interfaces* **13**(36), 43075–43084 (2021)
96. J. Fan, L. Qian, Quantum dot patterning by direct photolithography. *Nat. Nanotechnol.* **17**, 906–907 (2022)
97. J. Yang, D. Hahm, K. Kim, S. Rhee, M. Lee, S. Kim, J.H. Chang, H.W. Park, J. Lim, M. Lee, H. Kim, J. Bang, H. Ahn, J.H. Cho, J. Kwak, B. Kim, C. Lee, W.K. Bae, M.S. Kang, High-resolution patterning of colloidal quantum dots via non-destructive, light-driven ligand crosslinking. *Nat. Commun.* **11**, 2874 (2020)
98. Y. Wang, I. Fedin, H. Zhang, D.V. Talapin, Direct optical lithography of functional inorganic nanomaterials. *Science* **357**, 385–388 (2017)
99. Y. Wang, J.-A. Pan, H. Wu, D.V. Talapin, Direct wavelength-selective optical and electron-beam lithography of functional inorganic nanomaterials. *ACS Nano* **13**(12), 13917–13931 (2019)
100. M.J. Kim, M. Lee, H. Min, S. Kim, J. Yang, H. Kweon, W. Lee, D.H. Kim, J.-H. Choi, D.Y. Ryu, M.S. Kang, B. Kim, J.H. Cho, Universal three-dimensional crosslinker for all-photopatterned electronics. *Nat. Commun.* **11**(1), 1520 (2020)
101. D. Hahm, J. Lim, H. Kim, J.-W. Shin, S. Hwang, S. Rhee, J.H. Chang, J. Yang, C.H. Lim, H. Jo, B. Choi, N.S. Cho, Y.-S. Park, D.C. Lee, E. Hwang, S. Chung, C. Kang, M.S. Kang, W.K. Bae, Direct patterning of colloidal quantum dots with adaptable dual-ligand surface. *Nat. Nanotechnol.* **17**, 952–958 (2022)
102. J. Ahn, H.J. Choi, J. Bang, G. Son, S.J. Oh, Ink-lithographic fabrication of silver-nanocrystal-based multi-axial strain gauge sensors through the coffee-ring effect for voice recognition applications. *Nano Convergence* **9**, 46 (2022)
103. H.-V. Han, H.-Y. Lin, C.-C. Lin, W.-C. Chong, J.-R. Li, K.-J. Chen, P. Yu, T.-M. Chen, H.-M. Chen, K.-M. Lau, H.-C. Kuo, Resonant-enhanced full-color emission of quantum-dot-based micro LED display technology. *Opt. Express* **23**, 32504–32515 (2015)
104. T.A. Cohen, D. Sharp, K.T. Kluherz, Y. Chen, C. Munley, R.T. Anderson, C.J. Swanson, J.J.D. Yoreo, C.K. Luscombe, A. Majumdar, D.R. Gamelin, J.D. Mackenzie, Direct patterning of perovskite nanocrystals on nanophotonic cavities with electrohydrodynamic inkjet printing. *Nano Lett.* **22**(14), 5681–5688 (2022)
105. B.H. Kim, M.S. Onses, J.B. Lim, S. Nam, N. Oh, H. Kim, K.J. Yu, J.W. Lee, J.-H. Kim, S.-K. Kang, C.H. Lee, J. Lee, J.H. Shin, N.H. Kim, C. Leal, M. Shim, J.A. Rogers, High-resolution patterns of quantum dots formed by electrohydrodynamic jet printing for light-emitting diodes. *Nano Lett.* **15**(2), 969–973 (2015)
106. J. Ahn, S. Jeon, H.K. Woo, J. Bang, Y.M. Lee, S.J. Neuhaus, W.S. Lee, T. Park, S.Y. Lee, B.K. Jung, H. Joh, M. Seong, J. Choi, H.G. Yoon, C.R. Kagan, S.J. Oh, Ink-Lithography for Property Engineering and Patterning of Nanocrystal Thin Films. *ACS Nano* **15**(10), 15667–15675 (2021)
107. T.-H. Kim, K.-S. Cho, E.K. Lee, S.J. Lee, J. Chae, J.W. Kim, D.H. Kim, J.-Y. Kwon, G. Amaratunga, S.Y. Lee, B.L. Choi, Y. Kuk, J.M. Kim, K. Kim, Full-colour quantum dot displays fabricated by transfer printing. *Nat. Photonics* **5**, 176–182 (2011)
108. T.-H. Kim, D.-Y. Chung, J. Ku, I. Song, S. Sul, D.-H. Kim, K.-S. Cho, B.L. Choi, J.M. Kim, S. Hwang, K. Kim, Heterogeneous stacking of nanodot monolayers by dry pick-and-place transfer and its applications in quantum dot light-emitting diodes. *Nat. Commun.* **4**, 2637 (2013)
109. M.K. Choi, J. Yang, K. Kang, D.C. Kim, C. Choi, C. Park, S.J. Kim, S.I. Chae, T.-H. Kim, J.H. Kim, T. Hyeon, D.-H. Kim, Wearable red–green–blue quantum dot light-emitting diode array using high-resolution intaglio transfer printing. *Nat. Commun.* **6**, 7149 (2015)
110. M. Shirayama, M. Kato, T. Miyadara, T. Sugita, T. Fujiseki, S. Hara, H. Kadowaki, D. Muratam M. Chikamatsu, and H. Fujiwara, Degradation mechanism of CH<sub>3</sub>NH<sub>3</sub>PbI<sub>3</sub> perovskite materials upon exposure to humid air, *J. Appl. Phys.* **119**, 115501 (2016).
111. C. Zou, C. Chang, D. Sun, K.F. Böhringer, L.Y. Lin, Photolithographic patterning of perovskite thin films for multicolor display applications. *Nano Lett.* **20**(5), 3710–3717 (2020)
112. W. Kim, S.-K. Kim, S. Jeon, J. Ahn, B.K. Jung, S.Y. Lee, C. Shin, T.-Y. Seong, S. Jeong, T.N. Ng, S.J. Oh, Patterning all-inorganic halide perovskite with adjustable phase for high-resolution color filter and photodetector arrays. *Adv. Funct. Mater.* **32**, 2111409 (2022)
113. J. I. Kwon, G. Park, G. H. Lee, J. H. Jang, N. J. Sung, S. Y. Kim, J. Yoo, K. Lee, H. Ma, M. Karl, T. J. Shin, M. H. Song, J. Yang, and M. K. Choi, Ultrahigh-resolution full-color perovskite nanocrystal patterning for ultrathin skin-attachable displays, *Sci. Adv.* **8** (43), (2022).

**Publisher's Note** Springer Nature remains neutral with regard to jurisdictional claims in published maps and institutional affiliations.

Springer Nature or its licensor (e.g. a society or other partner) holds exclusive rights to this article under a publishing agreement with the author(s) or other rightsholder(s); author self-archiving of the accepted manuscript version of this article is solely governed by the terms of such publishing agreement and applicable law.